

Next-to-leading order QCD predictions for W^+W^+jj production at the LHC

Tom Melia

Rudolf Peierls Centre for Theoretical Physics, 1 Keble Road, University of Oxford, UK
Email: t.melia1@physics.ox.ac.uk

Kirill Melnikov

Department of Physics and Astronomy, Johns Hopkins University, Baltimore, MD 21218, USA
Email: melnikov@pha.jhu.edu

Raoul Röntsch

Rudolf Peierls Centre for Theoretical Physics, 1 Keble Road, University of Oxford, UK
Email: r.rontsch1@physics.ox.ac.uk

Giulia Zanderighi

Rudolf Peierls Centre for Theoretical Physics, 1 Keble Road, University of Oxford, UK
Email: g.zanderighi1@physics.ox.ac.uk

ABSTRACT: Because the LHC is a proton-proton collider, sizable production of two positively charged W -bosons in association with two jets is possible. This process leads to a distinct signature of same sign high- p_\perp leptons, missing energy and jets. We compute the NLO QCD corrections to the QCD-mediated part of $pp \rightarrow W^+W^+jj$. These corrections reduce the dependence of the production cross-section on the renormalization and factorization scale to about ± 10 percent. We find that a large number of W^+W^+jj events contain a relatively hard third jet. The presence of this jet should help to either pick up the W^+W^+jj signal or to reject it as an unwanted background.

KEYWORDS: NLO Computations, QCD, Jets, Hadronic Colliders.

Contents

1. Introduction	1
2. Technical details	2
3. Results	5
4. Conclusion	10
A. Results for primitive amplitudes at a fixed phase space point	14

1. Introduction

The large energy and large luminosity of the LHC lead to sizable production cross-sections for multi-particle final states, including rather exotic ones. For example, one can produce a pair of positively charged W -bosons, in association with two jets $pp \rightarrow W^+W^+jj$. At $\sqrt{s} = 14$ TeV, the cross-section for this process is about 1 pb and therefore accessible. Leptonic decays of W -bosons give rise to two positively charged isolated leptons and missing energy, which is nearly a background-free signature.

The observation of this process is interesting in its own right, but there are other reasons to study it. Of particular importance are various physics cases for which $pp \rightarrow W^+W^+jj$ is a background process. Interestingly, such cases can be found both within and beyond the Standard Model. For example, it is possible to use same-sign lepton pairs to study *double parton scattering* at the LHC [1] in which case the single scattering process $pp \rightarrow W^+W^+jj$ is the background. Events with same-sign leptons, missing energy and two jets can also appear due to resonant slepton production which may occur in R -parity violating SUSY models [2] or in the case of diquark production [3] with subsequent decay of the diquark to e.g. pairs of top quarks. Similarly, one of the possible production mechanisms of the double-charged Higgs boson at the LHC has a signature of two same-sign leptons, missing energy and two jets [4].

At leading order in the perturbative expansion in QCD, the W^+W^+jj final state is produced in proton collisions by both electroweak (EW) and QCD mechanisms. Interference terms between these mechanisms are doubly suppressed due to the different color structure of the two processes; interference only occurs at sub-leading color and even then only when the quarks are all identical. We neglect these terms and consider the QCD process separately. The corresponding cross-sections scale as $\sigma_{\text{EW}} \sim \alpha_{\text{EW}}^4$ and $\sigma_{\text{QCD}} \sim \alpha_{\text{EW}}^2 \alpha_s^2$, where α_{EW} and α_s are electroweak and strong coupling constant respectively. Given the large hierarchy between strong and weak coupling constants, one expects $\sigma_{\text{QCD}} \gg \sigma_{\text{EW}}$, but this

turns out to be too naive. In reality, the production cross-section due to a gluon exchange is only about fifty percent larger than the production cross-section of $pp \rightarrow W^+W^+jj$ by electroweak mechanisms [1].

As we mentioned earlier, W^+W^+jj production is the background to a number of interesting beyond the Standard Model (BSM) physics processes. It is peculiar that NLO QCD corrections to some of these *signal* BSM processes were calculated, see e.g. Refs. [2, 3]. Also, the NLO QCD corrections to the *electroweak* production of W^+W^+jj were calculated recently in Ref. [5], but similar corrections to the QCD production of W^+W^+jj are unknown. There is a clear reason for this: the computation of NLO QCD corrections to the QCD-induced process $pp \rightarrow W^+W^+jj$ is more involved because $pp \rightarrow W^+W^+jj$ is a $2 \rightarrow 4$ process. As a result, the NLO QCD calculation for QCD-induced $pp \rightarrow W^+W^+jj$ requires dealing with one-loop six-point tensor integrals of relatively high rank, while for the EW-induced process this is not the case since at Born level there is no color exchange between the quark lines. Until very recently, theoretical methods for one-loop calculations were inadequate to handle computations of such a complexity, but the situation has changed dramatically in the past two years. Thanks to recent technical developments [6, 7, 8, 9, 10, 11, 12, 13, 14, 15], NLO QCD computations for such $2 \rightarrow 4$ processes as $pp \rightarrow W(Z) + 3$ jets, $pp \rightarrow t\bar{t} + b\bar{b}$, $q\bar{q} \rightarrow b\bar{b}b\bar{b}$ and $pp \rightarrow t\bar{t} + 2$ jets, have been performed during the *past* year [16, 17, 18, 19, 20, 21, 22, 23, 24, 25, 26]. Similar techniques should be applicable to NLO QCD computations of processes with several electroweak gauge bosons and jets, and $pp \rightarrow W^+W^+jj$ is an interesting example. We also note that the computation of NLO QCD corrections to $pp \rightarrow W^+W^+jj$ involves a small subset of amplitudes needed for the computation of NLO QCD corrections to $pp \rightarrow W^+W^-jj$, which is an important background to Higgs boson production in weak boson fusion.

The remainder of the paper is organized as follows. In Section 2 we briefly discuss technical aspects of the calculation. In Section 3 we describe the results. In Section 4 we present our conclusions. In the Appendix, numerical results for one-loop helicity amplitudes for $0 \rightarrow (\bar{q}_i W^+ q_j)(\bar{q}_k W^+ q_m)$ are given.

2. Technical details

In this Section, technical aspects of the computation are summarized. It is well-known that the computation of NLO QCD corrections to any process requires three ingredients – one-loop virtual corrections to a Born process, real emission corrections and the subtraction counter-terms for infra-red and collinear singularities. To compute the one-loop virtual corrections, we use the framework of generalized D -dimensional unitarity [13, 14], closely following and extending the implementation described in Ref. [27]. Because the one-loop virtual corrections are computed using unitarity cuts, an important ingredient for the computation of one-loop corrections are the tree-level helicity amplitudes $0 \rightarrow (\bar{q}_i W^+ q_j)(\bar{q}_k W^+ q_m) + g$. We compute those helicity amplitudes using Berends-Giele recursion relations [28]. Incidentally, these amplitudes are the ones that are needed to compute the real emission corrections to $pp \rightarrow W^+W^+jj$. The subtraction terms are calculated using the Catani-Seymour dipole formalism [29]. We employ the optimization of

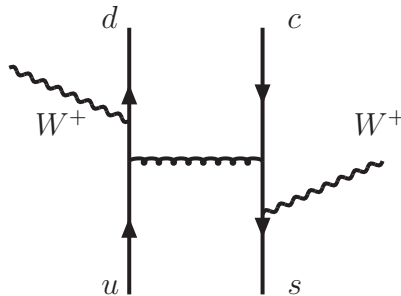


Figure 1: A typical Feynman diagram that contributes to QCD production of W^+W^+jj in hadron collisions at leading order in perturbative QCD.

the subtraction technique suggested in Ref. [30], where the subtraction is only performed if the kinematics of the event is close to either soft or collinear limit. Our implementation of the Catani-Seymour formalism closely follows the program MCFM [31]. In fact, we use the MCFM framework extensively to combine virtual and real emission corrections and the subtraction terms. Finally, we evaluate one-loop scalar integrals using the QCDloop library [32].

We now describe the computation in some detail. First, we point out that within the generalized unitarity framework, a basic object that needs to be calculated for each phase-space point is a one-loop helicity amplitude. To decouple color, helicity amplitudes are expressed through primitive amplitudes [33]. Those primitive amplitudes can be computed with the help of the color-stripped Feynman rules [33, 34, 35]. We note that, for the calculation of a given primitive amplitude, color-charged particles are ordered while all permutations of color-neutral particles must be considered, to achieve a gauge-invariant result. For our purposes, this implies that the ordering of the W^+ bosons is not fixed and we have to account for all possible insertions of the W^+ bosons. Fortunately, given the fact that both of the two W bosons have the same charge, this is a relatively minor complication since two W -bosons can not couple to the same quark line. Throughout the paper we treat the top quark as infinitely heavy, while all other quarks are taken to be massless. We do not consider final state top production as this leads to a different experimental signature. Top quarks therefore only contribute through fermion loops. While it is possible to deal with massive particles in the loop with D-dimensional unitarity [36, 37], we choose to neglect these effects since the momentum transfer through the fermion loop is far below the threshold for top pair production. This is consistent with the treatment of parton distribution functions, which use β_0 with five flavours in the evolution of α_s .

We now give the decomposition of the scattering amplitudes in terms of primitive amplitudes. We begin with the tree-level process $0 \rightarrow \bar{u} d \bar{c} s + (W^+ \rightarrow e^+ \nu_e) + (W^+ \rightarrow \mu^+ \nu_\mu)$, where we fix the flavor structure, for definiteness and treat the Cabibbo-Kobayashi-

Maskawa matrix as diagonal. The amplitude for this process reads

$$A^{\text{tree}}(\bar{u}, d, \bar{c}, s; e^+, \nu_e, \mu^+, \nu_\mu) = g_s^2 \left(\frac{g_W}{\sqrt{2}} \right)^4 P_{W^+}(s_{e^+\nu_e}) P_{W^+}(s_{\mu^+\nu_\mu}) \\ \times \left(\delta_{id i_{\bar{c}}} \delta_{is i_{\bar{u}}} - \frac{1}{N_c} \delta_{id i_{\bar{u}}} \delta_{is i_{\bar{c}}} \right) A_0(\bar{u}, d, \bar{c}, s), \quad (2.1)$$

where $g_{s,W}$ are the strong and weak coupling constants, respectively, quark color indices are indicated explicitly, $N_c = 3$ is the number of colors, and lepton labels in the right hand side of Eq.(2.1) are suppressed. Also, we use the W^+ propagators with a Breit-Wigner form in Eq.(2.1)

$$P_{W^+}(s) \equiv \frac{s}{s - M_W^2 + i\Gamma_W M_W}. \quad (2.2)$$

Finally, to account for leptonic decays $W^+ \rightarrow l^+(q_1)\nu_l(q_2)$ in Eq.(2.1), we replace the polarization vector of the outgoing W^+ bosons by

$$\epsilon_-^\mu(q_1, q_2) = \frac{\bar{u}(q_2)\gamma_\mu\gamma_-v(q_1)}{(q_1 + q_2)^2}, \quad \gamma_- = \frac{1 - \gamma_5}{2}. \quad (2.3)$$

A typical diagram that contributes to the amplitude $A_0(\bar{u}, d, \bar{c}, s)$ is shown in Fig. 1.

The computation of real emission corrections requires the scattering amplitude for $0 \rightarrow \bar{u} d \bar{c} s + g + (W^+ \rightarrow e^+\nu_e) + (W^+ \rightarrow \mu^+\nu_\mu)$. The amplitude for this process is written in terms of primitive amplitudes

$$A^{\text{tree}}(\bar{u}, d, \bar{c}, s, g; e^+, \nu_e, \mu^+, \nu_\mu) = g_s^3 \left(\frac{g_W}{\sqrt{2}} \right)^4 P_{W^+}(s_{e^+\nu_e}) P_{W^+}(s_{\mu^+\nu_\mu}) \\ \times \left[T_{is i_{\bar{u}}}^a \delta_{id i_{\bar{c}}} A_0(\bar{u}, d, \bar{c}, s, g) + T_{id i_{\bar{c}}}^a \delta_{is i_{\bar{u}}} A_0(\bar{u}, d, g, \bar{c}, s) \right. \\ \left. + \frac{1}{N_c} (T_{id i_{\bar{u}}}^a \delta_{is i_{\bar{c}}} A_0(\bar{u}, g, d, \bar{c}, s) + T_{is i_{\bar{c}}}^a \delta_{id i_{\bar{u}}} A_0(\bar{u}, d, \bar{c}, g, s)) \right]. \quad (2.4)$$

Again, in the right hand side of this equation the lepton labels are suppressed. Finally, the one-loop amplitudes required for this calculation can be written as

$$A^{\text{one-loop}}(\bar{u}, d, \bar{c}, s; e^+, \nu_e, \mu^+, \nu_\mu) = \\ g_s^4 \left(\frac{g_W}{\sqrt{2}} \right)^4 P_{W^+}(s_{e^+\nu_e}) P_{W^+}(s_{\mu^+\nu_\mu}) [\delta_{id i_{\bar{c}}} \delta_{is i_{\bar{u}}} A_1 + \delta_{id i_{\bar{u}}} \delta_{is i_{\bar{c}}} A_2]. \quad (2.5)$$

The color-ordered amplitudes $A_{1,2}$ can be expressed through the primitive amplitudes shown in Fig. 2. The relations read

$$A_1 = \left(N_c - \frac{2}{N_c} \right) A_a(\bar{u}, d, \bar{c}, s) - \frac{2}{N_c} A_a(\bar{u}, d, s, \bar{c}) \\ - \frac{1}{N_c} A_b(\bar{u}, s, \bar{c}, d) - \frac{1}{N_c} A_c(\bar{u}, s, \bar{c}, d) + n_f A_d(\bar{u}, d, \bar{c}, s), \quad (2.6)$$

$$A_2 = \frac{1}{N_c^2} A_a(\bar{u}, d, \bar{c}, s) + \left(1 + \frac{1}{N_c^2} \right) A_a(\bar{u}, d, s, \bar{c}) \\ + \frac{1}{N_c^2} A_b(\bar{u}, s, \bar{c}, d) + \frac{1}{N_c^2} A_c(\bar{u}, s, \bar{c}, d) - \frac{n_f}{N_c} A_d(\bar{u}, d, \bar{c}, s). \quad (2.7)$$

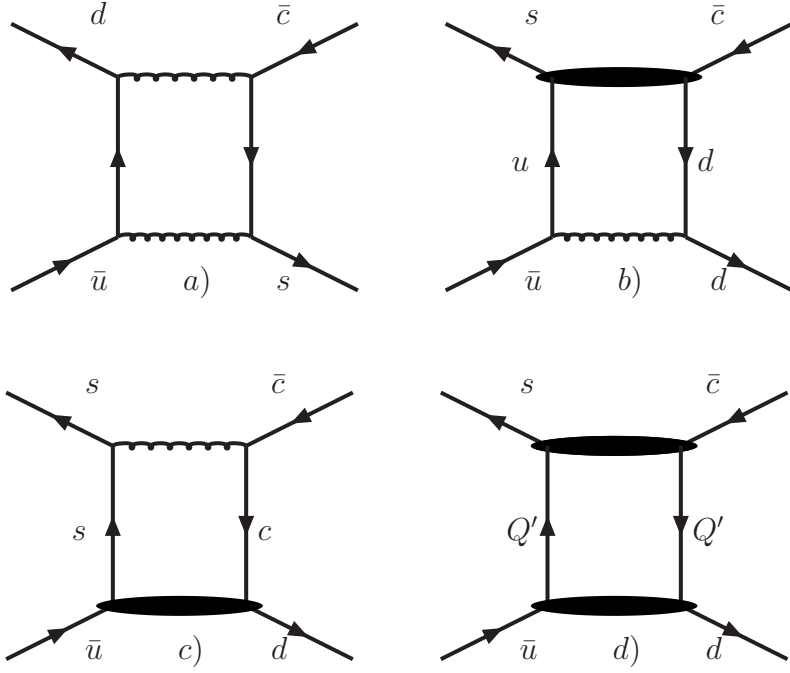


Figure 2: Parent diagrams for one-loop primitive amplitudes for $0 \rightarrow \bar{u}d\bar{c}s + W^+W^+$. Shaded areas represent dummy lines which can not be cut. W^+ bosons are not shown. Quarks Q' do not couple to W -bosons.

Amplitudes with two adjacent quarks can be reduced to amplitudes where quarks and anti-quarks alternate using the C-parity relation

$$A_a(\bar{u}^{\lambda_u}, d^{\lambda_d}, s^{\lambda_s}, \bar{c}^{\lambda_c}) = -A_a(\bar{u}^{\lambda_u}, d^{\lambda_d}, \bar{s}^{\lambda_s}, c^{\lambda_c}), \quad (2.8)$$

where we explicitly indicate fermion helicities¹.

Amplitudes with two identical quarks and anti-quarks are obtained from the amplitudes shown above by anti-symmetrising quarks or anti-quarks and including the appropriate symmetry factors in the cross-section calculation. Finally, we note that numerical results for helicity amplitudes at a particular phase-space point are given in the Appendix.

3. Results

In this Section, we present the results of the calculation. We consider proton-proton collisions with the center-of-mass energy $\sqrt{s} = 14$ TeV. We require leptonic decays of the W -bosons and consider $e^+\mu^+\nu_e\nu_\mu$ final state. The W -bosons are on the mass-shell and we neglect quark flavour mixing. We note that if identical leptons in the final state are present, there are interference effects not included in our calculation. However, such interference effects force the W -bosons off the mass shell, so that their numerical importance is limited.

¹We note that the r.h.s. of Eq. (2.8) is non-zero, since once the helicities of the fermions are fixed, we implement the coupling of the W -bosons to fermions as a vector coupling.

Within this approximation, the cross-sections for same- and different-flavor production are related $\sigma(pp \rightarrow \mu^+\mu^+X) = \sigma(pp \rightarrow e^+e^+X) = 0.5 \sigma(pp \rightarrow e^+\mu^+X)$. This implies that the cross-section for the full flavor sum $e^+\mu^+ + e^+e^+ + \mu^+\mu^+$ can be obtained by multiplying our results by a factor two.

We impose standard cuts on lepton transverse momenta $p_{\perp,l} > 20$ GeV, missing transverse momentum $p_{\perp,\text{miss}} > 30$ GeV and charged lepton rapidity $|\eta_l| < 2.4$. We define jets using anti- k_\perp algorithm [38], with $\Delta R_{j_1j_2} = \sqrt{(\eta_{j_1} - \eta_{j_2})^2 + (\phi_{j_1} - \phi_{j_2})^2} = 0.4$ and, unless otherwise specified, with a transverse momentum cut $p_{\perp,j} = 30$ GeV on the two jets. The mass of the W -boson is taken to be $m_W = 80.419$ GeV, the width $\Gamma_W = 2.140$ GeV. W couplings to fermions are obtained from $\alpha_{\text{QED}}(m_Z) = 1/128.802$ and $\sin^2 \theta_W = 0.2222$. We use MSTW08LO parton distribution functions for leading order and MSTW08NLO for next-to-leading order computations, corresponding to $\alpha_s(M_Z) = 0.13939$ and $\alpha_s(M_Z) = 0.12018$ respectively [39]. We do not impose lepton isolation cuts. All results discussed below apply to the QCD production $pp \rightarrow W^+W^+jj$; the electroweak contribution to this process is ignored. Note, however, that at next-to-leading order, QCD and electroweak production processes start to interfere and the separation of the two production mechanisms is not as clean as it is at leading order.

We point out that, because a massive gauge boson is produced from each fermion line, the cross-section for the process $pp \rightarrow W^+W^+jj$ remains finite *even* if the requirement that two jets are observed is lifted. Hence, we can consider the production of same-sign gauge bosons in association with n jets $pp \rightarrow W^+W^+ + n$ jets, where $n = 0, 1, 2$ or $n \geq 2$. It is useful to consider different jet multiplicities separately because, depending on the number of jets, backgrounds to $pp \rightarrow W^+W^+ + n$ jets change. Also, if we are interested in $pp \rightarrow W^+W^+ + n$ jets as a potential background to New Physics processes, it is helpful to know how jetty this process is.

We begin by showing in Fig. 3 the dependence of the production cross-sections for $pp \rightarrow e^+\mu^+\nu_e\nu_\mu + n$ jets on the renormalization and factorization scales, which we set equal to each other. We show results for the following four processes *i*) $pp \rightarrow W^+W^+ + \geq 2$ jets; *ii*) $pp \rightarrow W^+W^+ + 2$ jets; *iii*) $pp \rightarrow W^+W^+ + 1$ jet; and *iv*) $pp \rightarrow W^+W^+ + 0$ jets. The total inclusive cross-section is then given by the sum of the two-jet inclusive cross-section, the one-jet exclusive cross-section and the zero-jet exclusive cross-section. The difference between inclusive and exclusive two jet cross-sections shows how often W^+W^+ is produced in association with three, rather than two, jets.

It is clear from Fig. 3 that leading order cross-sections for all jet multiplicities monotonically increase with the decrease of the renormalization/factorization scales. This behavior is driven by the dependence of the leading order cross-section on the square of the strong coupling constant; the factorization scale dependence is minor. It follows from Fig. 3 that when cross-sections are calculated at next-to-leading order in perturbative QCD, they show significantly reduced scale dependence. For example, considering the range of scales $50 \text{ GeV} \leq \mu \leq 400 \text{ GeV}$, we find the two-jet inclusive cross-section to be $\sigma^{\text{LO}} = 2.7 \pm 1.0$ fb at leading order and $\sigma^{\text{NLO}} = 2.44 \pm 0.18$ fb at next-to-leading order. The forty percent scale uncertainty at leading order is reduced to less than ten percent at NLO. We observe similar stabilization of the scale dependence for the 0- and 1-jet exclusive multiplicities.

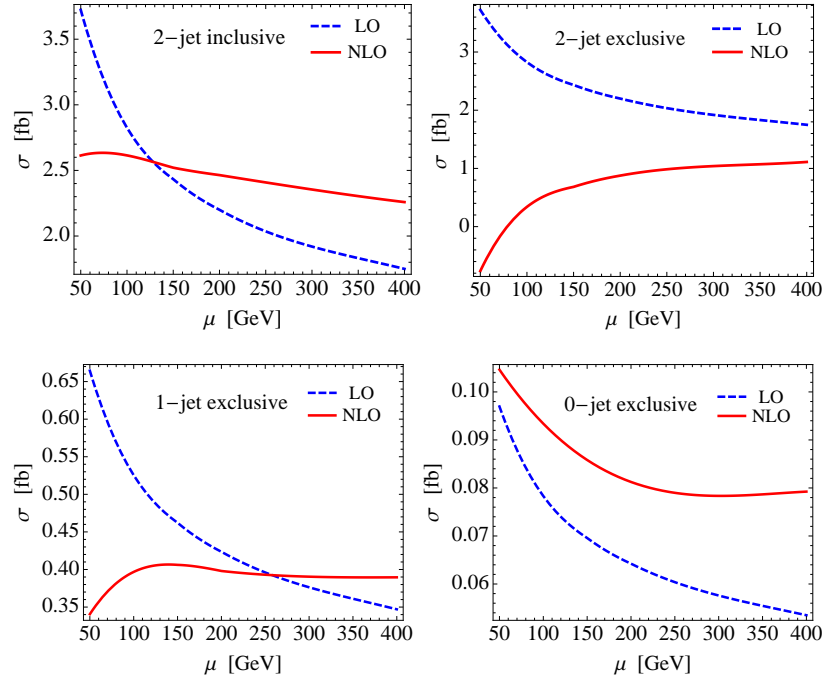


Figure 3: The dependence on factorization and renormalization scales of cross-sections for $pp \rightarrow e^+ \mu^+ \nu_e \nu_\mu + n$ jets, $n = 0, 1, 2$ at leading and next-to-leading order in perturbative QCD. We set the two scales equal to each other $\mu_F = \mu_R = \mu$.

Combining these cross-sections we obtain a total NLO cross-section of about 2.90 fb for $pp \rightarrow e^+ \mu^+ \nu_e \nu_\mu$ inclusive production. This implies about 60 $e^+ \mu^+ + e^+ e^+ + \mu^+ \mu^+$ events per year at the LHC with 10 fb^{-1} annual luminosity. While this is not a gigantic number, such events will have a very distinct signature, so they will definitely be seen and it will be possible to study them.

On the other hand, it is apparent from Fig. 3 that there is quite a dramatic change in the two-jet *exclusive* cross-section. At leading order, there is no difference between the exclusive and inclusive cross-sections, but this difference appears at NLO. With $\Delta R_{jj} = 0.4$ and a transverse momentum jet cut of 30 GeV, the two-jet exclusive cross-section is only about 0.7 fb at $\mu = 150$ GeV; if the scale is decreased to about 80 GeV, the two-jet exclusive cross-section becomes negative. One can argue that this is the consequence of the fact that the 30 GeV jet transverse momentum cut is too small for the convergence of the perturbative expansion of the two-jet exclusive cross-section. However, it is not fully clear how to make this explanation compatible with the reasonable perturbative stability of the zero-jet and the one-jet exclusive cross-sections for the same value of the jet transverse momentum cut. In Fig. 4 we show the inclusive and exclusive cross-sections for $pp \rightarrow e^+ \mu^+ \nu_e \nu_\mu + 2$ jets at next-to-leading order in perturbative QCD, in dependence on the jet p_\perp cut. We set the factorization and renormalization scales equal to each other $\mu_R = \mu_F = \mu$, and vary the scale μ in the range $100 \text{ GeV} \leq \mu \leq 200 \text{ GeV}$. It is clear that for a jet cut of 40 – 50 GeV, the scale dependence of the exclusive two-jet cross-section is relatively small, while for

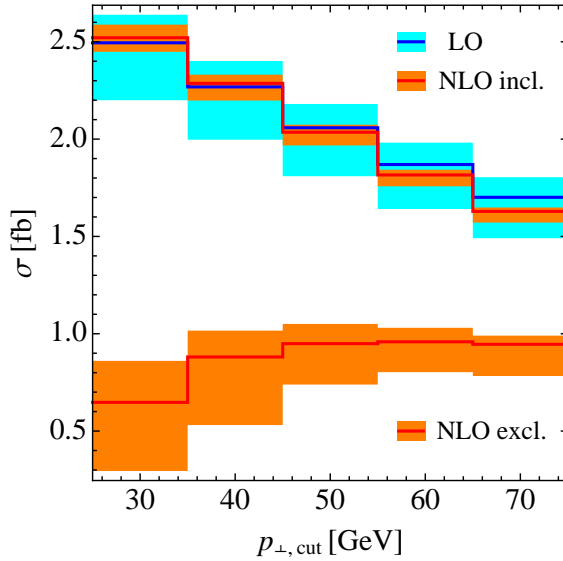


Figure 4: The dependence on the jet p_{\perp} cut of the two-jet inclusive and two-jet exclusive cross-sections for $pp \rightarrow e^+ \mu^+ \nu_e \nu_{\mu} + 2$ jets at leading and next-to-leading order in perturbative QCD. We show scale uncertainty bands, for values of the renormalization and factorization scales set to a common value μ , which is varied in the interval $100 \text{ GeV} \leq \mu \leq 200 \text{ GeV}$. Results for $\mu = 140 \text{ GeV}$ are shown as solid lines.

the 30 GeV jet cut, the scale dependence increases strongly. The results displayed in Fig. 4 suggest that, whatever the exact value of the exclusive two-jet cross-section is, it is significantly smaller than the two-jet inclusive cross-section. This smallness implies that quite a large fraction of events in $pp \rightarrow e^+ \mu^+ \nu_e \nu_{\mu} + \geq 2$ jets have a relatively hard third jet. This effect remains present, although less pronounced, for larger values of R . This feature may be useful for rejecting contributions of $pp \rightarrow W^+ W^+ jj$ when looking for multiple parton scattering.

We now turn to the discussion of kinematic distributions. Unless explicitly stated otherwise, we will consider two-jet inclusive processes. A glance at Fig. 3 suggests that NLO QCD corrections to jet cross-sections are small if the renormalization and factorization scales are set to $\mu = 150 \text{ GeV}$. Indeed, for $\mu = 150 \text{ GeV}$, two-jet inclusive leading and next-to-leading order cross-sections nearly coincide $\sigma_{\text{LO}} = 2.4 \text{ fb}$ and $\sigma_{\text{NLO}} = 2.5 \text{ fb}$, so that the NLO QCD corrections change the leading order cross-sections by less than five percent. In the plots that follow, we show the scale uncertainty bands for $50 \text{ GeV} \leq \mu \leq 400 \text{ GeV}$ and predictions for $\mu = 150 \text{ GeV}$, for leading and next-to-leading order distributions.

The transverse momentum distributions of the hardest and next-to-hardest jets, as well as the distribution of the scalar sum of the transverse momenta of all jets and charged leptons and the missing transverse momentum in the event are shown in the first three pane of Fig. 5. It is clear from Fig. 5 that jets in $pp \rightarrow W^+ W^+ jj$ are hard; a typical transverse momentum of the hardest jet is close to 100 GeV and the transverse momentum of the next-to-hardest jet is close to 40 GeV. While no major changes in kinematic distributions

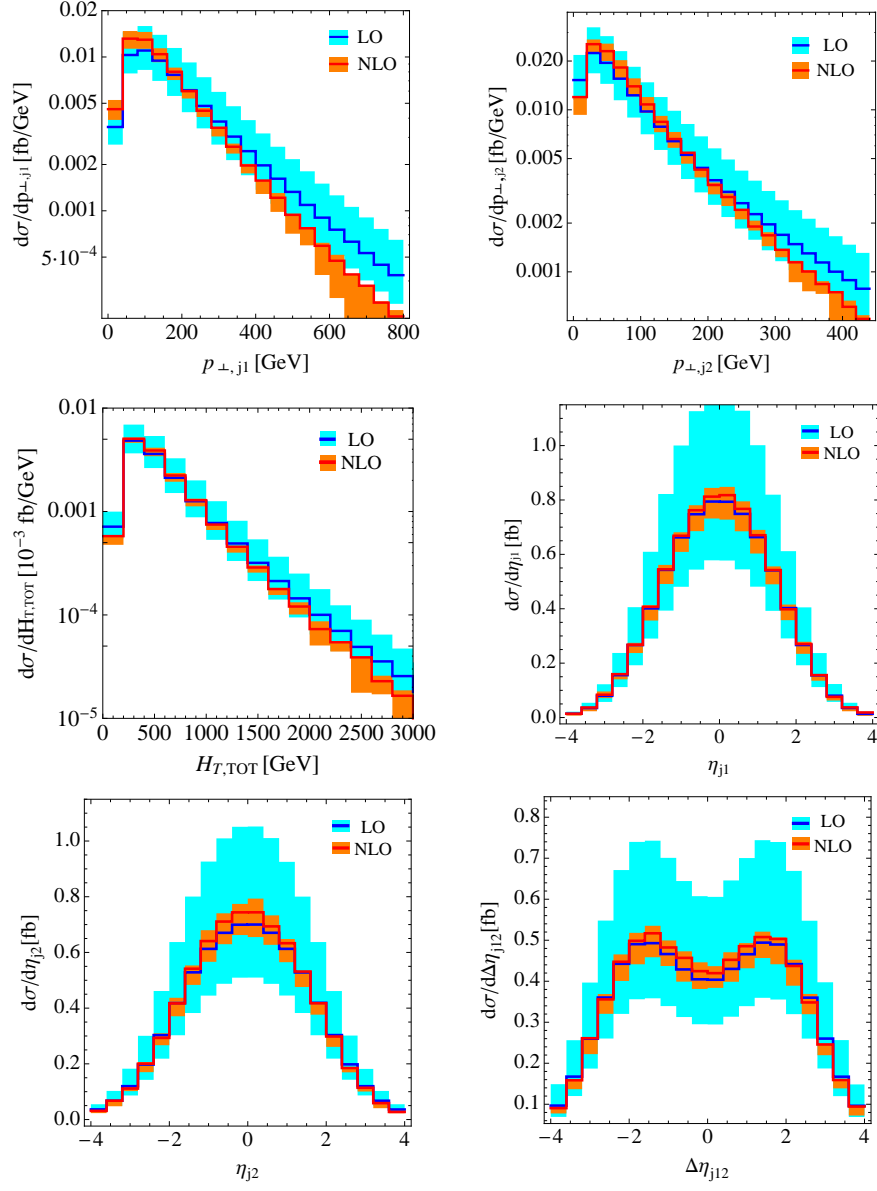


Figure 5: Kinematic distributions of the two hardest jets in the process $pp \rightarrow e^+ \mu^+ \nu_e \nu_\mu + 2 \text{ jets}$ at leading and next-to-leading order in perturbative QCD for inclusive two-jet events. The bands show renormalization and factorization scale uncertainty, for $50 \text{ GeV} \leq \mu \leq 400 \text{ GeV}$. Solid lines show leading and next-to-leading order predictions for $\mu = 150 \text{ GeV}$. We use $H_{T,\text{TOT}} = \sum_j p_{\perp,j} + p_{\perp}^{e^+} + p_{\perp}^{\mu^+} + p_{\perp}^{\text{miss}}$.

occur when NLO QCD corrections are calculated, some shape changes are apparent from Fig. 5. Indeed, the NLO QCD transverse momenta distributions of the hardest and next-to-hardest jet show a characteristic depletion at large values of $p_{\perp,j}$. One reason this change occurs is because a constant, rather than a dynamical, renormalization scale is used in our leading order calculation. As was emphasized many times recently, the choice

of dynamical renormalization scales in leading order computations may affect shapes of kinematic distributions in a manner similar to NLO QCD corrections [5, 20, 23, 40]. The shapes of rapidity distributions of the hardest and next-to-hardest jets, as well as the distribution of the rapidity differences between hardest and next-to-hardest jets, shown in the next three pane, remain very similar to the shapes of leading order distributions, once the NLO QCD corrections are included. On the other hand, scale dependencies of rapidity distributions are reduced dramatically.

We now turn to lepton and missing transverse momentum distributions. In Fig. 6 we show the charged lepton transverse momentum distribution, the missing transverse momentum distribution, the distributions of the charged lepton rapidity and of the rapidity difference of the two leptons, as well as the distributions of the invariant mass of the two charged leptons and the transverse mass of the two W -bosons ². Lepton kinematic distributions are affected by the QCD radiative corrections in a similar way to the jet kinematic distributions. We observe that transverse momentum distributions become softer while shapes of rapidity distributions are unaffected. Distributions of dilepton invariant mass and the transverse mass of the W -bosons become softer as well. It is also interesting to look at the angular distributions of the charged leptons. In Fig. 7 the angular distance $\Delta R_{lj} = \sqrt{(\eta_l - \eta_j)^2 + (\phi_l - \phi_j)^2}$ between a charged lepton of fixed flavor (e^+ or μ^+) and the hardest (next-to-hardest) jet is displayed, as well as the distribution of the relative azimuthal angle of the two charged leptons. Although distributions of angular distances between leptons and jets are broad, they peak at $\Delta R_{lj} \approx 3$ for both hardest and next-to-hardest jets. NLO QCD effects do not change this conclusion but, interestingly, they make the angular distance between next-to-hardest jet and the charged lepton somewhat *larger* at next-to-leading order. The distribution of the relative azimuthal angle of the two charged leptons becomes less peaked at $\Delta\phi_{l+l+} = \pi$, although the two leptons still prefer to be back to back. It is interesting to remark that, if the two same sign leptons are produced through a double-parton scattering mechanism, their directions are not correlated. Hence, yet another possibility to reduce the single-scattering-background is to cut on the relative azimuthal angle between the two leptons.

4. Conclusion

In this paper, we presented the computation of NLO QCD corrections to the QCD-mediated process $pp \rightarrow W^+W^+jj$ at the LHC. In spite of the fact that this is a $2 \rightarrow 4$ process, the computation of NLO QCD corrections is relatively straightforward, thanks to spectacular developments in technology of NLO QCD computations in recent years [6, 7, 8, 9, 10, 11, 12, 13, 14, 15]. We note that NLO QCD corrections to electroweak-mediated $pp \rightarrow W^+W^+jj$ process were recently calculated in Ref. [5].

²Since neutrinos are not observed, it is impossible to reconstruct the true transverse mass of the pair of the two W -bosons. We follow Ref.[41] and define $m_{\perp,WW}^2 = (E_{\perp,l+l+} + \tilde{E}_{\perp,\text{miss}})^2 - (\mathbf{p}_{\perp,l+l+} + \mathbf{p}_{\perp,\text{miss}})^2$, where the missing transverse energy $\tilde{E}_{\perp,\text{miss}}$ is reconstructed from the missing transverse momentum using the invariant mass of the charged lepton system $\tilde{E}_{\perp,\text{miss}} = \sqrt{\mathbf{p}_{\perp,\text{miss}}^2 + m_{l+l-}^2}$.

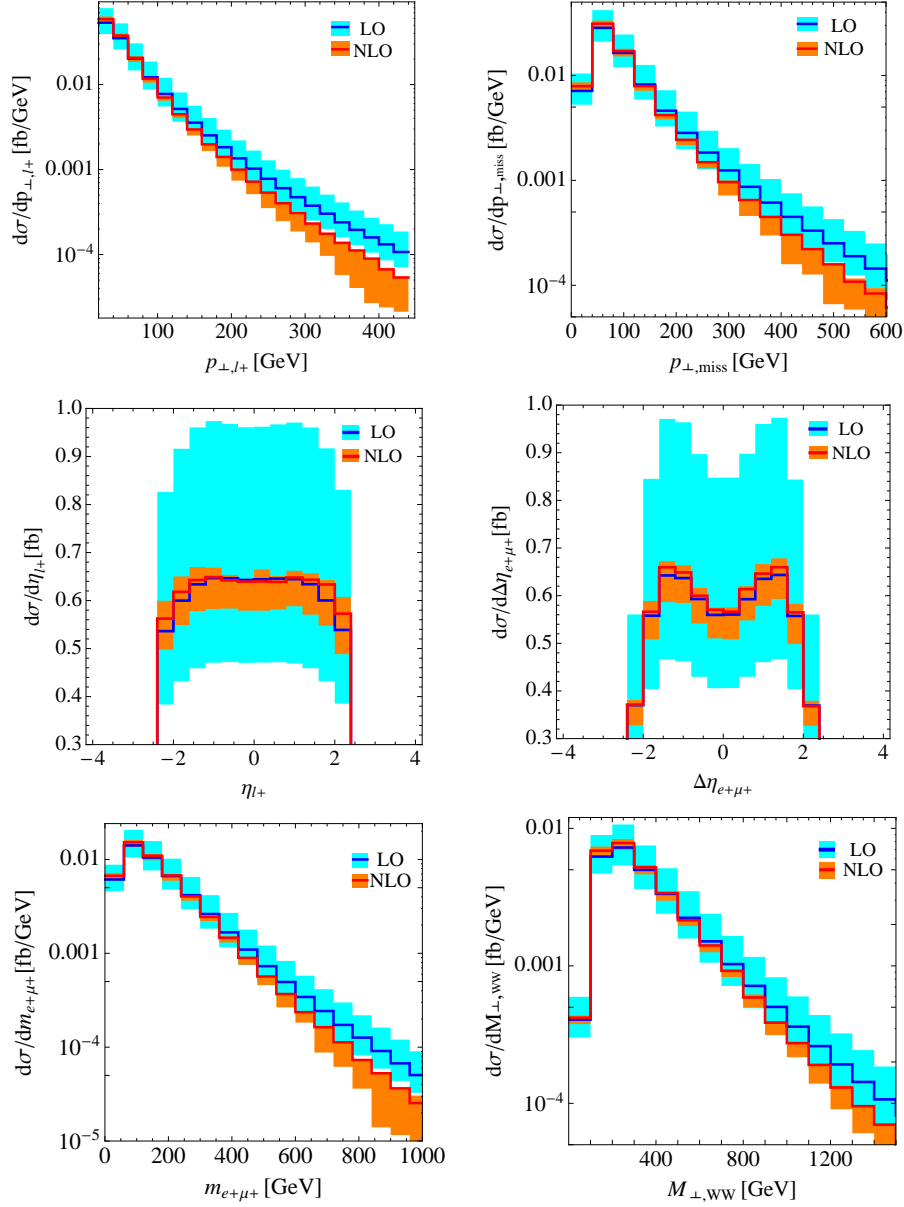


Figure 6: Kinematic distributions of charged leptons and missing energy in $pp \rightarrow e^+ \mu^+ \nu_e \nu_\mu + n$ jets at leading and next-to-leading order in perturbative QCD for inclusive two-jet events. The bands show renormalization and factorization scale uncertainty, for $50 \text{ GeV} \leq \mu \leq 400 \text{ GeV}$. Solid lines show leading and next-to-leading order predictions for $\mu = 150 \text{ GeV}$.

The production of two same-sign W -bosons in association with two jets is a background to studies of double-parton scattering, as well as to a number of beyond the Standard Model physics processes. The NLO QCD corrections to $pp \rightarrow W^+ W^+ jj$ reduce the scale dependence to about ten percent. An interesting feature of $pp \rightarrow W^+ W^+ jj$ is that perturbative QCD is applicable even if the observation of the two jets is not demanded. This opens up the possibility to study QCD radiative corrections to $pp \rightarrow W^+ W^+ + n$ jets where the num-

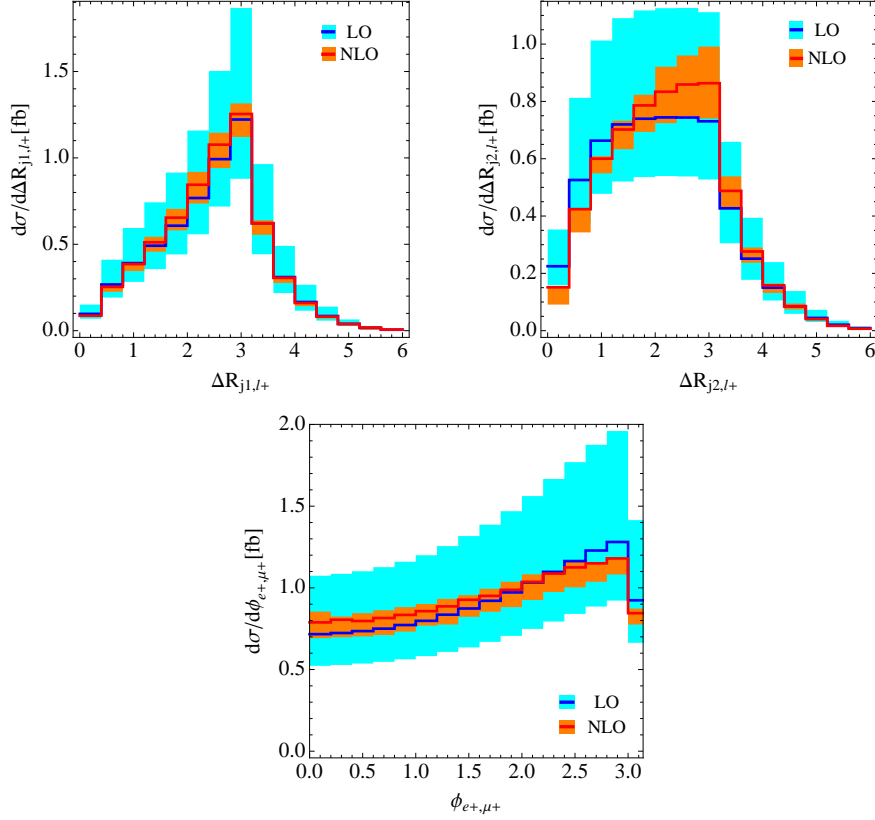


Figure 7: Angular kinematic distributions in the process $pp \rightarrow e^+\mu^+\nu_e\nu_\mu + 2$ jets at leading and next-to-leading order in perturbative QCD for inclusive two-jet events. The bands show renormalization and factorization scale uncertainty, for $50 \text{ GeV} \leq \mu \leq 400 \text{ GeV}$. Solid lines show leading and next-to-leading order predictions for $\mu = 150 \text{ GeV}$.

ber of jets can be zero, one and two. At next-to-leading order, the final state with three jets also appears. We have studied QCD corrections to processes with various jet multiplicities and observed reasonable behavior of the perturbative expansion for two-jet inclusive, and one- and zero-jet exclusive processes. The situation with the two-jet exclusive cross-section is less satisfactory. As follows from Fig. 4, the two-jet exclusive cross-section is about fifty percent of the inclusive cross-section. Since at leading order exclusive and inclusive two-jet cross-sections coincide, the NLO QCD correction is large. In addition, there is significant residual scale uncertainty in the prediction for the exclusive two-jet cross-section which is smaller than, but comparable to, the leading order scale dependence. We believe that these results suggest that nearly fifty percent of all events in $pp \rightarrow e^+\mu^+\nu_e\nu_\mu + \geq 2$ jets contain a relatively hard third jet. It may be possible to use this effect in designing selection or suppression criteria for W^+W^+jj final state. We have also studied a variety of kinematic distributions and showed that no dramatic shape changes occur.

As a final comment, we point out that the production of two *negatively* charged W -bosons at the LHC is also possible, at a rate which is about forty percent of the W^+W^+ production [1]. We can use our set up to compute NLO QCD corrections to $pp \rightarrow W^-W^-jj$

using charge conjugation and parity reversal [5]. To this end, if we are interested in $pp \rightarrow e^- \mu^- \bar{\nu}_e \bar{\nu}_\mu jj$, we can do a calculation for $\bar{p}\bar{p} \rightarrow e^+ \mu^+ \nu_e \nu_\mu jj$, treat the final state leptons as if they are positively charged and reverse the momentum directions for parity-odd distributions.

Acknowledgments We thank Anna Kulesza, Ezio Maina and Dieter Zeppenfeld for comments on the relative magnitude of the QCD- and electroweak-mediated contributions to $pp \rightarrow W^+ W^+ jj$. We acknowledge useful conversations with Ed Berger, Zoltan Kunszt and Paolo Nason. We thank Valentin Hirschi and Thomas Reiter for pointing out an error in the Tables. During the work on this paper, we have benefited from the hospitality extended to us by Aspen Center for Physics and CERN Theory Division. This research is supported by the NSF under grant PHY-0855365, by the start up funds provided by Johns Hopkins University and by the British Science and Technology Facilities Council.

A. Results for primitive amplitudes at a fixed phase space point

In this Appendix we give numerical results for all primitive amplitudes needed to reconstruct the one-loop amplitudes in Eq. (2.5) at a particular phase space point. The momenta (E, p_x, p_y, p_z) , in GeV, are chosen to be

$$\begin{aligned}
k_1(\bar{u}) &= (-500.000000000000, -500.000000000000, 0.00000000000000, 0.00000000000000), \\
k_2(d) &= (-500.000000000000, 500.000000000000, 0.00000000000000, 0.00000000000000), \\
k_3(\bar{c}) &= (54.2314070117999, -31.1330162081798, -7.92796656791140, 43.6912823611163), \\
k_4(s) &= (214.488870161418, -27.0607980217775, -98.5198083786150, 188.592247959949), \\
k_5(e^+) &= (85.5312248384887, -8.22193223977868, 36.1637837682033, -77.0725048002414), \\
k_6(\nu_e) &= (181.428811610043, -57.8599829481937, -171.863734086635, -5.61185898481311), \\
k_7(\mu^+) &= (82.8493010774356, -65.9095476235891, -49.8952157196287, 5.51413360058664), \\
k_8(\nu_\mu) &= (381.470385300815, 190.185277041519, 292.042940984587, -155.113300136598).
\end{aligned} \tag{A.1}$$

Because the W -bosons couple only to left-handed fermions and right-handed anti-fermions, all helicities in the following are fixed, so that $\{\bar{u}, d, \bar{c}, s, e^+, \nu_e, \mu^+, \nu_\mu\}$ have helicities $\{+, -, +, -, +, -, +, -\}$. Below we tabulate numerical results for the primitive tree and one-loop amplitudes at the phase-space point given in Eq. (A.1). In Table 1 we display tree-level amplitudes and ratios of *unrenormalized* one-loop amplitudes to tree-amplitudes

$$r_i = \frac{1}{c_\Gamma} \frac{A_i}{A_0} \tag{A.2}$$

where $c_\Gamma = \frac{\Gamma(1+\epsilon)\Gamma^2(1-\epsilon)}{(4\pi)^{2-\epsilon}\Gamma(1-2\epsilon)}$ and the A_i are defined through equations (2.5) - (2.7). We use $\mu_R = 80$ GeV; it enters our calculation through the usual modification of the loop integration measure $\int d^4k \rightarrow \mu_R^{2\epsilon} \int d^Dk$ in dimensional regularization. The one-loop amplitudes are calculated in the four-dimensional helicity scheme [42]. In Table 2 we give the ratio S

$$S = \frac{4\pi}{\alpha_s} \frac{\text{Re}(A^{\text{one-loop}} A^{\text{tree}*})}{|A^{\text{tree}}|^2} \tag{A.3}$$

of amplitudes summed over spin and color. Note that *all* unrenormalized virtual amplitudes (including fermion loops) contribute to $A^{\text{one-loop}}$.

Amplitude	$1/\epsilon^2$	$1/\epsilon$	ϵ^0
$A_0(\bar{u}, d, \bar{c}, s)$			$-7.488599 - i 17.47659$
$r_a(\bar{u}, d, \bar{c}, s)$	-2.000000	$5.580909 + i 0.000000$	$11.010146 + i 14.39329$
$r_a(\bar{u}, d, s, \bar{c})$	-2.000000	$6.634395 + i 0.000000$	$-16.15227 - i 7.909865$
$r_b(\bar{u}, s, \bar{c}, d)$	-1.000000	$3.551457 - i 3.141593$	$-2.605243 + i 9.184110$
$r_c(\bar{u}, s, \bar{c}, d)$	-1.000000	$-2.092934 - i 3.141593$	$-1.237780 - i 9.355851$
$r_d(\bar{u}, s, \bar{c}, d)$		$-0.666667 + i 0.000000$	$1.431296 - i 2.305401$

Table 1: Numerical results for the primitive tree-level amplitude $A_0(\bar{u}, d, \bar{c}, s)$, in units of $10^{-11} \text{ GeV}^{-4}$ and the ratios of primitive one-loop amplitudes r_i .

Ratio	$1/\epsilon^2$	$1/\epsilon$	ϵ^0
$S(\bar{u}, d, \bar{c}, s)$	-5.333333	13.62554	23.35965

Table 2: Numerical results for the ratio of spin and color summed amplitudes $S(\bar{u}, d, \bar{c}, s)$.

References

- [1] A. Kulesza and W. J. Stirling, Phys. Lett. B **475**, 168 (2000);
E. Maina, JHEP **0909**, 081 (2009);
J. R. Gaunt, C. H. Kom, A. Kulesza and W. J. Stirling, hep-ph/1003.3953.
- [2] H. K. Dreiner, S. Grab, M. Krämer and M. K. Trenkel, Phys. Rev. D **75**, 035003 (2007).
- [3] T. Han, I. Lewis and T. McElmurry, JHEP **1001**, 123 (2010).
- [4] See e.g. J. Maalampi and N. Romanenko, Phys. Lett. B **532**, 202 (2002) and references therein.
- [5] B. Jager, C. Oleari and D. Zeppenfeld, Phys. Rev. D **80**, 034022 (2009).
- [6] A. Denner and S. Dittmaier, Nucl. Phys. B **734**, 62 (2006).
- [7] T. Binoth, J. P. Guillet, G. Heinrich, E. Pilon and C. Schubert, JHEP **0510**, 015 (2005).
- [8] R. Britto, F. Cachazo and B. Feng, Nucl. Phys. B **725**, 275 (2005).
- [9] R. Britto, F. Cachazo and B. Feng, Phys. Lett. B **611**, 167 (2005).
- [10] D. Forde, Phys. Rev. D **75**, 125019 (2007).
- [11] G. Ossola, C. G. Papadopoulos and R. Pittau, Nucl. Phys. B **763**, 147 (2007).
- [12] G. Ossola, C. G. Papadopoulos and R. Pittau, JHEP **0805**, 004 (2008).
- [13] R. K. Ellis, W. T. Giele and Z. Kunszt, JHEP **0803**, 003 (2008).
- [14] W. T. Giele, Z. Kunszt and K. Melnikov, JHEP **0804**, 049 (2008).
- [15] C. F. Berger *et al.*, Phys. Rev. D **78**, 036003 (2008).
- [16] A. Bredenstein, A. Denner, S. Dittmaier and S. Pozzorini, Phys. Rev. Lett. **103**, 012002 (2009).
- [17] A. Bredenstein, A. Denner, S. Dittmaier and S. Pozzorini, JHEP **1003**, 021 (2010).

- [18] G. Bevilacqua, M. Czakon, C. G. Papadopoulos, R. Pittau and M. Worek, JHEP **0909**, 109 (2009).
- [19] C. F. Berger *et al.*, Phys. Rev. Lett. **102**, 222001 (2009).
- [20] C. F. Berger *et al.*, Phys. Rev. D **80**, 074036 (2009).
- [21] R. K. Ellis, K. Melnikov and G. Zanderighi, JHEP **0904**, 077 (2009).
- [22] R. Keith Ellis, K. Melnikov and G. Zanderighi, Phys. Rev. D **80**, 094002 (2009).
- [23] K. Melnikov and G. Zanderighi, Phys. Rev. D **81**, 074025 (2010).
- [24] T. Binoth, N. Greiner, A. Guffanti, J.-Ph. Guillet, T. Reiter, J. Reuter, Phys. Lett. B **685**, 293, (2010).
- [25] G. Bevilacqua, M. Czakon, C. G. Papadopoulos and M. Worek, Phys. Rev. Lett. **104**, 162002 (2010).
- [26] C. F. Berger *et al.*, arXiv:1004.1659 [hep-ph].
- [27] R. K. Ellis, W. T. Giele, Z. Kunszt, K. Melnikov and G. Zanderighi, JHEP **0901**, 012 (2009).
- [28] F.A. Berends and W. T. Giele, Nucl. Phys. B **306**, 759 (1988).
- [29] S. Catani and M. H. Seymour, Nucl. Phys. B **485**, 291 (1997) [Erratum-ibid. B **510**, 503; (1998)].
- [30] Z. Nagy and Z. Trocsanyi, Phys. Rev. D **59**, 014020 (1999) [Erratum-ibid. D **62**, 099902 (2000)]; Z. Nagy, Phys. Rev. D **68**, 094002 (2003).
- [31] J. M. Campbell and R.K. Ellis, Phys. Rev. D **62**, 114012 (2000). The MCFM program is publicly available from <http://mcfm.fnal.gov>.
- [32] R.K. Ellis and G. Zanderighi, JHEP **0802**, 002 (2008).
- [33] Z. Bern, L. J. Dixon and D. A. Kosower, Nucl. Phys. B **437**, 259 (1995).
- [34] Z. Bern, L. J. Dixon and D. A. Kosower, Nucl. Phys. B **513**, 3 (1998).
- [35] Z. Bern, L. Dixon and D. Kosower, Ann. Rev. Nucl. Part. Sci. **46**, 109 (1996).
- [36] R. K. Ellis, W. T. Giele, Z. Kunszt and K. Melnikov, Nucl. Phys. B **822**, 270 (2009).
- [37] K. Melnikov and M. Schulze, Nucl. Phys. B **840**, 129 (2010).
- [38] M. Cacciari, G. P. Salam and G. Soyez, JHEP **0804**, 063 (2008).
- [39] A. D. Martin, W. J. Stirling, R. S. Thorne and G. Watt, Eur. Phys. J. C **63**, 189 (2009).
- [40] Contribution by S. Höche, J. Huston, D. Maitre, J. Winter and G. Zanderighi to T. Binoth *et al.* “The SM and NLO multileg working group: Summary report”, arXiv:1003.1241[hep-ph].
- [41] A. Alves, O. Eboli, T. Plehn and D. Rainwater. Phys. Rev. D **69**, 075005 (2004).
- [42] Z. Bern and D. A. Kosower, Nucl. Phys. B **379**, 451 (1992); Z. Bern, A. De Freitas, L. J. Dixon and H. L. Wong, Phys. Rev. D **66**, 085002 (2002).